LEGIBILITY NOTICE

A major purpose of the Technical Information Center is to provide the broadest dissemination possible of information contained in DOE's Research and Development Reports to business, industry, the academic community, and federal, state and local governments.

Although a small portion of this report is not reproducible, it is being made available to expedite the availability of information on the research discussed herein.

ORNL/TM--11032

DE89 007876

Engineering Physics and Mathematics

Inclusion of Correlations in the Empirical Selection of Intranuclear Cascade Nucleons From High-Energy Hadron-Nucleus Collisions

F. S. Alsmiller and R. G. Alsmiller, Jr.

DATE PUBLISHED — January 1989

NOTICE: This document contains information of a preliminary nature. It is subject to revision or correction and therefore does not represent a final report.

Prepared by the
OAK RIDGE NATIONAL LABORATORY
Oak Ridge, Tennessee 37831
operated by
MARTIN MARIETTA ENERGY SYSTEMS, INC.
for the
U.S. DEPARTMENT OF ENERGY
under contract DE–AC05–84OR21400

CONTENTS

LIST OF FIGURES

ABSTRACT

The very high energy (5 GeV to 20 TeV) hadron-nucleus differential particle production model found in the Monte Carlo transport code FLUKA87 has been adapted for inclusion in the transport code HETC88. The empirical selection of intranuclear cascade nucleons has been modified to provide simple correlations with the randomly selected number of hadron-nucleon collisions. A standard method of calculating the excitation energy of the compound nucleus preceding an added evaporation step by assuming the particles are produced in a one-dimensional nuclear well is applied. This method, coupled with the above correlations, leads to improved correlations of the excitation energy with the A and Z of the compound nucleus, and then to greatly improved distributions of the residual nuclei following evaporation. The frequency distributions of low energy ($\beta < .7$) charged particles show good agreement with experiment for 200 GeV protons incident on emulsions. Average multiplicities of shower and grey particles after evaporation for protons and pions incident on several elements are also compared with experiment.

1. INTRODUCTION

Particle production spectra and multiplicities from high-energy (hundreds and thousands of GeV) hadron-nucleus collisions are of particular interest in shielding calculations for accelerators such as the proposed Superconducting Super Collider,[1,2] and also in high energy calorimeter calculations of energy deposition and fluctuations. A multi-chain fragmentation model using quark physics and generating exclusive events has been implemented into a cross section code, EVENTQ, embedded in the transport code FLUKA by J. Ranft et al. (see Ref. 3 and references included therein). This model is based on work of A. Capella et al. (see Ref. 4 and included references). An intranuclear cascade secondary nucleon component was also included in EVENTQ to account for particles produced by lower energy secondary collisions. These nucleons are not, as yet, calculated by a direct cascade calculation similar to that used at energies below 3.5 GeV in the transport code HETC82.[5,6]

In the available versions of EVENTQ[7] the cascade nucleons are chosen first and are fitted by simple procedures giving the total kinetic energy to be used (the same in each collision), and the nucleon energy spectra to be sampled from. No correlation of these nucleons with the number of collisions in the high energy model is provided. The particles are emitted isotropically. Energy is conserved, but not momentum, except on the average. A fixed amount of energy is also set aside to account for the excitation and kinetic energies of the compound nucleus.

A modified EVENTQ was developed specifically for incorporation into the high energy transport codes HETC82[5] and HETC88[6] and comparisons with experiment have been obtained with both codes. In particular, unlike FLUKA, very low energy particles (<50 MeV) are followed, making evaporation calculations necessary.

Earlier calculations[8] of the excitation and kinetic energies of the compound nuclei before evaporation provided correlations of these energies with the number of particles escaping an assumed one-dimensional nuclear well. However, the residual nuclei distributions following evaporation did not agree with experiment because a large number of cascade nucleons could be chosen inside the well when the number of high energy collisions was small (one or more). Many of these escaped the well, adding their potential energies to the energies of the compound nucleus. Excitation energies that peaked at values too large, coupled with compound nuclei atomic mass number distributions that did not peak at atomic mass numbers near that of the target nucleus led to incorrect A,Z distributions for the final residual nuclei. This also meant that the evaporation particle energy spectra and multiplicities could be incorrect.

A very simple method of including the required cascade particle correlations is described in Section 2.1. The total kinetic energy given to cascade nucleons in individual collisions was correlated with the number of high energy hadron collisions which were chosen in advance. In this way, the number of cascade nucleons, and in particular, the number of grey tracks, were correlated with the number of high-energy collisions. That a correspondence of this kind should exist was pointed out by Babecki and Nowak.[9] The kinetic energy given to cascade nucleons was modified to bring the calculated average multiplicities of grey charged particles ($.25 < \beta \leq .7$) into better agreement with the experimental data of Faessler[10] at 150 GeV. The

energy spectra and direction cosines of the selected nucleons inside the nuclear well are still taken to be those given by Ranft. The details of the nuclear well model are given in Section 2.2.

Calculated average multiplicities for 50 and 150 GeV protons colliding with several nuclei are compared with the experimental data of Faessler[10] in Section 3.1. Also, the frequency distributions of grey and black particles resulting from 200 GeV protons and pions in emulsions are compared with the data of Babecki and Nowak.[9] In Section 3.2., the mass yield distributions for 29 GeV proton-silver collisions are compared with the data of Katcoff et al.,[11] and the mass yield distributions for 300 GeV proton-silver collisions are compared with the data of Porile et al.[12]

In Section 3.3., the rapidity distribution for 200 GeV proton-argon collisions is compared with the data of DeMarzo et al.[13]

2. INTRANUCLEAR CASCADE NUCLEONS

2.1 CORRELATION OF TOTAL CASCADE KINETIC ENERGY WITH COLLISIONS INSIDE THE WELL

A typical frequency distribution of hadron-hadron collisions in the high energy calculation for 200 GeV/c protons incident on emulsions is shown in Fig. 1. This was sampled from a cumulative distribution adapted by Ranft from the work of Nelsson and Stenlund.[14] It is parameterized by an average number of collisions, $\bar{\nu}$, and limited to a maximum of 13 collisions. One collision is always initiated by the valence quarks of the original projectile and the remaining N_{sea} collisions by pi-zero-like mesons composed of sea quarks. The total number of collisions is $N_{coll} = N_{sea} + 1$.

In the new EVENTQ, (currently, EVENTQ.HETC.88), these collisions are chosen in advance, along with the type of target nucleon and its Fermi kinetic energy; N_{prot} and N_{neut} are the number of target protons and neutrons, respectively. Then

$$\begin{aligned} A_{com} &= A_T - N_{prot} - N_{neut}, \\ Z_{com} &= Z_T - N_{prot}, \end{aligned} \tag{1}$$

are computed initially, where A_T and Z_T are atomic mass number and charge number of the target nucleus.

The total kinetic energies, $E_{co}(E, A_T)$, to be expended in cascade neutron and proton kinetic energies are taken from FLUKA87 and are given in Ref. 15; E is the incident particle kinetic energy. These energies are somewhat larger for neutrons than for protons, so that the cascade neutron multiplicity exceeds that of the cascade protons.

The average energy E_{co} is then multiplied by a new fraction, $Fract\,(A_T, IJ)$, where IJ denotes the type of incident hadron, e.g., a meson or a hadron with baryon number unequal to zero. Tables of these fractions are given in Ref. 15. They were chosen to make the final average multiplicities of grey particles agree with the experimental data of Faessler,[10] which is largely independent of E for $E \geq$ 30 GeV. The value of $Fract$ for silver, $A_T = 107$, is 0.874 for baryons and 0.656 for mesons, with smaller values as A_T decreases.

The correlation is introduced by calculation of an additional factor, P_E, so that the actual total cascade kinetic energy available for each collision, E_c, is given by

$$\begin{aligned} E_c &= P_E * Fract * E_{co}, \\ P_E &= cnsea/(\bar{\nu} - 1.0 - ext), \\ ext &= 0.25, \\ (N_{sea} - ext - 0.5) &< cnsea \leq (N_{sea} - ext + 0.5). \end{aligned} \tag{2}$$

where $cnsea$ is chosen randomly from a histogram of unit width about the value $N_{sea} - ext$. Thus, the average of P_E over many collisions for a given target and initial energy, e.g., over a distribution such as that shown in Fig. 1, should be unity, (the histogram average of $cnsea$ is $N_{sea} - ext$ and the collision average of N_{sea} is $\bar{\nu}$

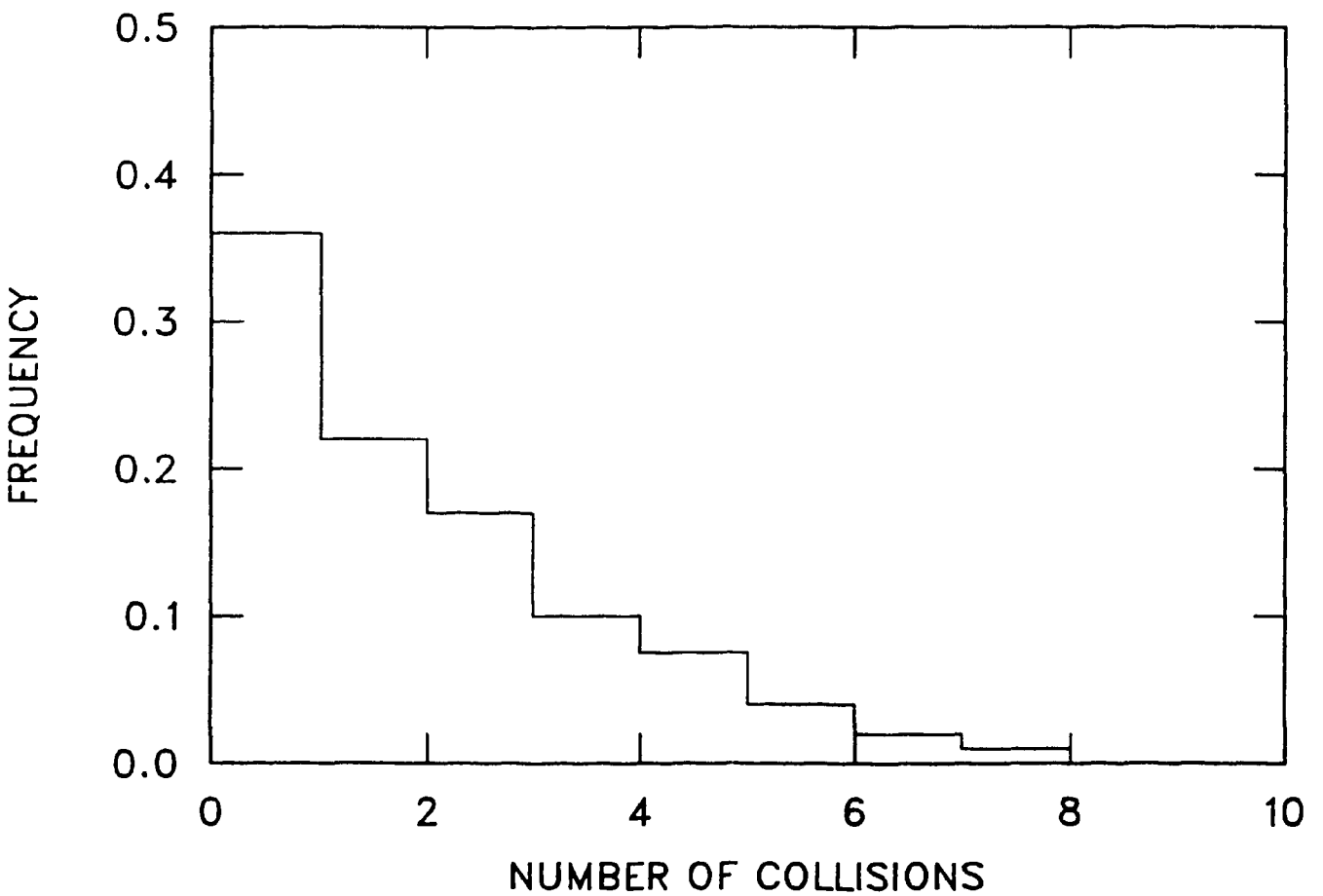

Figure 1. Frequency distribution of hadron-hadron collisions in 200 GeV proton-emulsion collisions.

- 1.0). However, Fig. 1 shows that $N_{sea} = 0$ for many collisions, which are purely valence collisions. Since a negative value of P_E is not wanted, *cnsea* is set equal to zero when negative. Then, with $ext = .25$, $cnsea > 0$ occurs only 25% of the time when $N_{sea} = 0$. However, if the denomnator of P_E is negative or zero, the value $P_E = 1.0$ is used. Thus, the average value of P_E ranges from 1.0 to 1.2, which is one reason a renormalizing fraction, *Fract*, is needed. A second reason is the need to not deplete the small A_T nuclei.

The value of *ext* was chosen to give a crude approximation to quasi-elastic scattering cases, and other reactions leading to only two or three secondaries, which contribute to the high values of the final residual nuclei A-distributions near A_T (see Figs. 8 and 9).

In order to obtain this peak, it was also necessary to retain a carryover feature of the original EVENTQ, in which any proton cascade kinetic energy not used up in one collision is added to E_c for protons in the next collision, and the same for neutrons.

Selection of intranuclear cascade particles and their kinetic energies begins with a neutron, followed by a proton, then a neutron, etc. After each selection, A_{com} and Z_{com} are diminished so that

$$\begin{aligned} A_{com} &\geq Z_{com} + 3 \\ Z_{com} &\geq 3 \end{aligned} \tag{3}$$

The limiting conditions are necessary to insure the compound nucleus is not completely depleted when the target is a light element such as carbon or oxygen. Alternate selection continues until the energy available for protons is used up; then only neutrons are chosen until the neutron energy is used up, or the limiting conditions on A_{com} and Z_{com} are met. After the one-dimensional cutoff nuclear well is introduced to cutoff some emergent particles (mostly black cascade nucleons), any compound nucleus with $A_{com} \leq Z_{com}$ or $Z_{com} \leq 0$ is rejected, and the collision redone.

The kinetic energy distributions for cascade neutrons and protons are unchanged from those used in FLUKA87, and are given in Ref. 15. Prior to the selection of cascade nucleons, an amount of energy, TV, is set aside to account for compound nucleus energies. However, TV = 0.0 is used when the particles are assumed to be born inside a cutoff nuclear well, because the well is used to provide nuclear excitation.

Energy and momentum conservation inside the wells are given by the free space expressions found in the original EVENTQ, except for $\Delta E_{o,well}$,

$$\begin{aligned} E_{nuc} &= E_{KE} + m_o \\ &= E_o + \Delta E_{o,well} - TV - \sum_{c=1}^{N_c} (E'_c - m_c) \\ \vec{P}_{nuc} &= [E_{KE}(E_{KE} + 2m_o)]^{1/2}\, \vec{P}_o / P_o \end{aligned} \tag{4}$$

where E_{nuc} and $\vec{P}_{nuc}$ are the energy and momentum of the projectile entering the fragmentation model; m_o is its mass and E_{KE} its kinetic energy, with P_{nuc}

calculated from them and taken in the direction of the incoming projectile. For this projectile, E_o and $\vec{P}_o$ are the incoming initial energy and momentum; E_o is incremented by $\Delta E_{o,well}$ if it is not a meson, with $\Delta E_{o,well}$ equal to the nuclear well depth for the incoming particle. Also, a $\Delta \vec{P}_{o,well}$ can be calculated to satisfy kinematics. The number of cascade nucleons is N_c, with m_c, E'_c and $\vec{P}'_c$ the mass, total energy, and momentum of a cascade nucleon. Only the kinetic energies of the cascade nucleons are subtracted from the initial energy, so their mass energies must be assumed initially present. Errors exist in the momentum conservation at this stage, partly because the cascade nucleons are chosen isotropically, but mainly because they are chosen first, i.e., if their momentum is subtracted from $\vec{P}_o + \Delta \vec{P}_{o,well}$, the result is not $\vec{P}_{nuc}$ of Eq. (4).

The Fermi total energies and momenta of the target nucleons in Ranft's collision well are assumed initially present, so are added to E_{nuc} and $\vec{P}_{nuc}$ and then expended in high energy secondary particle production. Here, $KE_{F,k}$, m_k, and $\vec{P}_{F,k}$ are the Fermi kinetic energy, mass, and momentum of a target nucleon.

$$\begin{aligned} E_{nuc} + \sum_{k=1}^{N_{coll}} (KE_{F,k} + m_k) &= \sum_{s=1}^{N'_s} E'_{s,coll} + E_{err} \\ \vec{P}_{nuc} + \sum_{k=1}^{N_{coll}} \vec{P}_{F,k} &= \sum_{s}^{N'_s} \vec{P}'_{s,coll} + \vec{P}_{err} \end{aligned} \tag{5}$$

The energy and momentum of the N'_s high energy particles are $E'_{s,coll}$ and $\vec{P}'_{s,coll}$. The errors in energy and momentum conservation, E_{err} and $\vec{P}_{err}$, are not zero at this stage for several reasons, including the use of single precision in HETC, and some systematic errors. Some, but not all, of the systematic errors in FLUKA82 were eliminated in FLUKA87; a few more that were corrected in HETC82 were again corrected in HETC88.

The error E_{err} was first computed from Eq. (5) and then removed by dividing it equally among the kinetic energies of the high energy secondaries. The momenta are then recomputed, keeping directions unchanged. (Of course, overall momentum conservation using the cascade particles still fails by as much as several GeV.) This procedure is followed because the excitation plus kinetic energies of the compound nuclei before evaporation are calculated using energy conservation and need to be correct to within at least 20 MeV. Some tables of errors in energy and momentum conservation before this renormalization are given in Ref. 15.

Conservation of charge, baryon number, and strangeness is carried out in the high-energy hadron-hadron collision model, HADEVT. Using the fact that the sea collisions are initiated by mesons with zero charge, baryon number, and strangeness, similar conservation laws can be written for all the secondaries produced before the cutoff well is applied. Thus, N_{bar} is the total baryon number for all secondaries, including intranuclear cascade particles,

$$N_{bar} = N_{coll} + N_c + I_{bar,o} = \sum_{s=1}^{N'_s+N_c} Ibar_s. \tag{6}$$

where $I_{bar,o}$ is the baryon number of the incident particle and $Ibar_s$ the same for secondary particle, s. Of course, $Ibar = 0$ for mesons, +1 for baryons, and -1 for antibaryons.

It is clear that N_c is now correlated with the number of high-energy collisions, N_{coll}, because the total kinetic energy expended in creating the cascade nucleons was correlated with N_{coll}. Then, the total number of all secondaries inside the well, $N'_s + N_c$, is correlated with N_{coll}, and so is N_{bar}.

In the absence of a well, the compound nucleus, atomic mass number, A_c and Z_c charge number, are calculated at this point by baryon number and charge conservation,

$$\begin{aligned} A_C &= A_T + Ibar_o - N_{bar}; \\ Z_C &= Z_T + Z_o - N_{chg}; \end{aligned} \tag{7}$$

where

$$N_{chg} = \sum_{s=1}^{N'_s+N_c} Z_s = Z_o + \sum_{c=1}^{N_c} Z_c + \sum_{k=1}^{N_{coll}} Z_k.$$

and Z_s is the charge of secondary s, Z_o the charge of incident projectile, Z_c the charge of a cascade particle, and Z_k the charge of a target nucleon. The difference $A_T - A_C$ is now correlated with the number of high-energy collisions.

2.2 THE NUCLEAR WELLS AND COMPOUND NUCLEUS ENERGIES

The idea of nuclear wells has been implemented in the Monte Carlo intranuclear cascade code, BERT,[16] which is a part of HETC for nucleons with kinetic energies less than 3.5 GeV and for pions with kinetic energies less than 2.5 GeV. A nuclear well was used by Ranft[17] when Fermi kinetic energies (different for neutrons and protons) were assumed present initially for the target nucleons in the high energy collisions. However, Ranft did not use cutoff wells or Coulomb barriers to be applied to particles escaping the nucleus. This is partially because of the philosophy that high energy particles may exist as part of jets or complex fragments inside the nucleus and actually not be formed until after a certain delay time has elapsed, e.g., until they are outside the nucleus. On the other hand, the delay time is short enough for lower energy particles so that they are formed inside the nucleus and do collide again, providing the intranuclear cascade nucleons. These supposedly are formed inside the well, and give up energy upon escaping to the compound nucleus, which then exists in an excited state.

The purpose of the cutoff wells is just this: to provide variable correlated nuclear excitation energies that will lead to correct mass number distributions, and to reduce the multiplicity of escaping low energy nucleons, because they will be replaced by evaporation particles.

In order to have approximate energy conservation for the potentials, it was decided to assume potential energies corresponding to the left side of Eq. (6) are present initially and to make the secondary potential energies zero for mesons and for antibaryon pairs, insofar as it is possible to identify these. Of course, in a self-consistent model, the remaining potential energies should be computed from the maximum Fermi energies used by Ranft for the N_{coll} collisions. This was not done

because these collision Fermi wells were found to be too deep to provide correct excitation energies and multiplicities. Changing them would reduce the energy available for the high energy collisions and the multiplicity results for these and was not done.

The energies, E_s, of the secondary particles escaping the well (these now include intranuclear cascade particles) are decreased by an amount V_s equal to the appropriate cutoff well depth calculated from a degenerate Fermi gas. That is

$$\begin{aligned} V_s &= 0.0 && \text{; mesons} \\ &= KE_{F,max,p} + BE && \text{; charged baryons and antibaryons} \\ &= KE_{Fmax,n} + BE && \text{; neutral baryons and antibaryons} \\ &= 0.0 && \text{; baryon} - \text{antibaryon pairs} \\ BE &= 7.0\,MeV \end{aligned} \tag{8}$$

with $\Delta E_{o,well} = V_s$ for the incident particle in Eq. (4) and BE is an average binding energy.

The nuclear radius, r, in the Fermi gas calculation is given in Fermi's by

$$\begin{aligned} r &= r_o A_T^{1/3} \\ r_o &= 1.3 \end{aligned} \tag{9}$$

Then, the maximum Fermi momenta are $P_{F,max}$ (in MeV/c)

$$\begin{aligned} P_{F,max} &= An * [Z_T/A_T]^{1/3} && \text{; protons} \\ &= An * [(A_T - Z_T)/A_T]^{1/3} && \text{; neutrons} \\ An &= 291.3 \quad \text{for } r_o = 1.3, \\ &= 400.0 \quad \text{for Ranft well.} \end{aligned} \tag{10}$$

The maximum Fermi kinetic energies are given by the usual relation:

$$KE_{F,max} = [P_{F,max}^2 + m_k^2]^{1/2} - m_k. \tag{11}$$

All escaping positively charged particles are also required to have a kinetic energy exceeding the well depth V_s plus a Coulomb barrier given by

$$\text{Coulmb} = 1.4412\, Z_T^{1/3}/r \ \text{ MeV}. \tag{12}$$

The total energy E_R of the residual compound nucleus before evaporation is given by energy conservation

$$\begin{aligned} E_R &= E_o + M_T - \sum_{s=1}^{N_{ecc}} E_s, \\ &= U_R + KE_R + M_R. \end{aligned} \tag{13}$$

where M_T and M_R are the mass of the target nucleus and the residual compound nucleus; N_{sec} is the number of escaping secondaries; U_R and KE_R are the excitation and kinetic energies of the compound nucleus. Subtracting V_s,

$$\sum_{s=1}^{N_{sec}} E_s = \sum_{s=1}^{N'_s} E'_{s,coll} + \sum_{c=1}^{N_c} E_c - \sum_{r=1}^{N_r} E'_{s,r} - \sum_{s}^{N_{sec}} V_s. \tag{14}$$

where N_r is the number of secondaries (including mesons) retained in the nucleus; $E'_{s,r}$ is the total energy of the retained particles.

It is possible to define an average binding energy in a history, $Beav$, using an analysis of the energy conservation in the modified EVENTQ. Let N_{bary} be the number of emitted baryons, omitting baryon pairs,

$$\begin{aligned} N_{bary} &= \sum_{s=1}^{N_{sec}} \mid Ibar_s \mid -2\, N_{pair}, \\ Beav &= \left[M_R + \sum_{c=1}^{N_c} m_c + \sum_{k=1}^{N_{coll}} m_k - \sum_{r=1}^{N_b} m_r - M_T \right] / N_{bary}. \end{aligned} \tag{15}$$

The masses M_R and M_T are computed using Wapstra[18] mass tables; m_r is the mass of a retained particle; N_b is the number of retained baryons or antibaryons. N_{pair} is the number of emitted pairs; a pair is assumed (somewhat incorrectly) to be emitted every time an antibaryon is emitted, except for the case of an incident antibaryon.

The average value of $Beav$ generally ranges from 1-12 MeV depending upon the values of E and A_T, but $Beav$ itself shows very wide variations. Nevertheless, it is clear that both N_{bary} and $Beav$ are correlated with N_{coll}, since N_c and N_b both are.

Using energy conservation inside the well, with Eqs. 4, 5, 7, 8, gives an alternate expression for the sum of excitation and kinetic energies of the residual compound nucleus,

$$\begin{aligned} U_R + KE_R = {} & TV + E_{rr} \\ & + \sum_{s=1}^{N_{sec}} V_s - \Delta E_{o,well} \\ & - \sum_{k=1}^{N_{coll}} KE_{F,k} + \sum_{r=1}^{N_b} KE_r + \sum_{m=1}^{N_{mes}} E_m \\ & - N_{bary} * Beav. \end{aligned} \tag{16}$$

When the cutoff well is omitted,

$$U_R + KE_R = TV + E_{err} - \sum_{k=1}^{N_{coll}} KE_{F,k} - N_{bary} * Beav.$$

Here $TV + E_{crr} = 0$ when the well is used; $KE_{F,k}$ is the Fermi kinetic energy selected from the Ranft collision well for the target nucleon k; and KE_r is the kinetic energy of the r'th particle (excluding mesons) that is retained inside the nucleus because it does not have enough energy to escape from the well and the Coulomb barrier. N_{mes} is the number of retained positively charged mesons and E_m the total energy of the retained meson.

Care must be taken to keep $U_R + KE_R$ positive since the cutoff wells in V_s and collision wells in Fermi KE are not the same. The relatively deep collision well in the original EVENTQ causes the $KE_{F,k}$ terms to be large, thus augmenting the shower multiplicities, but use of the deep well for cutoff reduces the grey particle multiplicity significantly. The partition of U_R and KE_R is accomplished by using momentum conservation for the compound nucleus, even though momentum is not conserved inside the well.

$$\begin{aligned} \vec{P}_R &= \vec{P}_o - \sum_{s=1}^{N_{sec}} \vec{P}_s, \\ M_R^* &= [E_R^2 - P_R^2]^{1/2} \geq M_R, \\ KE_R &= E_R - M_R^*, \\ U_R &= M_R^* - M_R, \\ &= 0, \text{ if } M_R^* \leq M_R. \end{aligned} \tag{17}$$

The momentum P_s of the escaping secondaries is computed from the energy E_s and taken to have the same direction cosines as inside the well. Here, M_R^* is a defined excited mass of the compound nucleus given by the kinematic relation between E_R and P_R, and the kinetic energy KE_R is the difference between E_R and M_R^*; the excitation energy U_R is the difference between excited mass and rest mass of the compound nucleus.

The A and Z of the compound nucleus are now:

$$\begin{aligned} A_R &= A_T + Ibar_o - \sum_{s=1}^{N_{sec}} Ibar_s = A_C - \sum_{s=1}^{N_R} Ibar_s, \\ Z_R &= A_T + Z_o - \sum_{s=1}^{N_{sec}} Z_s = Z_C - \sum_{s=1}^{N_R} Z_s. \end{aligned} \tag{18}$$

Since many cascade nucleons are retained in the well, these distributions are more nearly peaked near A_T and Z_T than are those of Eq. (7).

Evaporation calculations were carried out using a previously developed evaporation model.[19] The A and Z of the final residual nucleus are now

$$\begin{aligned} A_{Res} &= A_R - N_{evap}, \\ Z_{Res} &= Z_R - Z_{evap}. \end{aligned} \tag{19}$$

where N_{evap} is the number of evaporation nucleons, with each nucleon in the light ions emitted being counted in N_{evap}; Z_{evap} is the total charge of the evaporation products.

3. RESULTS AND COMPARISONS WITH EXPERIMENT

3.1 MULTIPLICITIES

In Fig. 2 the calculated average multiplicities are compared with measured multiplicities taken from Faessler[10] of shower ($\beta > .7$) and grey ($.25 < \beta \leq .7$) particles. They are shown as functions of atomic mass number for 150- and 50-GeV/c incident protons. In Fig. 3 similar results are shown for 150- and 50-GeV/c incident π^+. Shower particles are given by the upper solid lines in these figures that are drawn through the experimental points to aid in interpreting the results. The error bars on the measured data in Figs. 2 and 3 are of the order of the size of the plotted points and the statistical errors on the calculated values are of the order of the size of the plotted points.

The high-energy cross section model in FLUKA87 includes diffractive collisions,[20] which occur randomly 30% of the time, for both valence and sea collisions. This diffractive effect has improved the agreement with experiment for shower particles produced by incident π^+ to some extent, as compared with previous results of Ranft and Ritter[21] and of Alsmiller et al.[8] for the EVENTQ82 program.

It has been well established for some time that the experimentally determined multiplicity of grey charged particles is independent of incident energy at the higher incident energies.[10] This fact is shown by the experimental data in Figs. 2 and 3 and is also reproduced very well by the new correlated calculational model over the entire range of energies and atomic mass number considered.

In Fig. 4 and Fig. 5 the calculated frequency distribution of grey and black charged particles after evaporation resulting from 200-GeV protons in nuclear emulsion are compared with the experimental data of Babecki and Nowak.[9] Similar comparisons are given in Figs. 6 and 7 for 200 GeV incident positively charged pions. The calculation used the composition of dry Ilford G_5 emulsions[22] given in Table 1. In the figure, the calculated and experimental multiplicities obtained from distributions are also given.

Table 1
Emulsion Composition

Element	Wt. in g/cm^3
Silver	2.025
Bromine	1.496
Iodine	0.026
Carbon	0.30
Hydrogen	0.049
Oxygen	0.20
Sulfur	0.011
Nitrogen	0.073

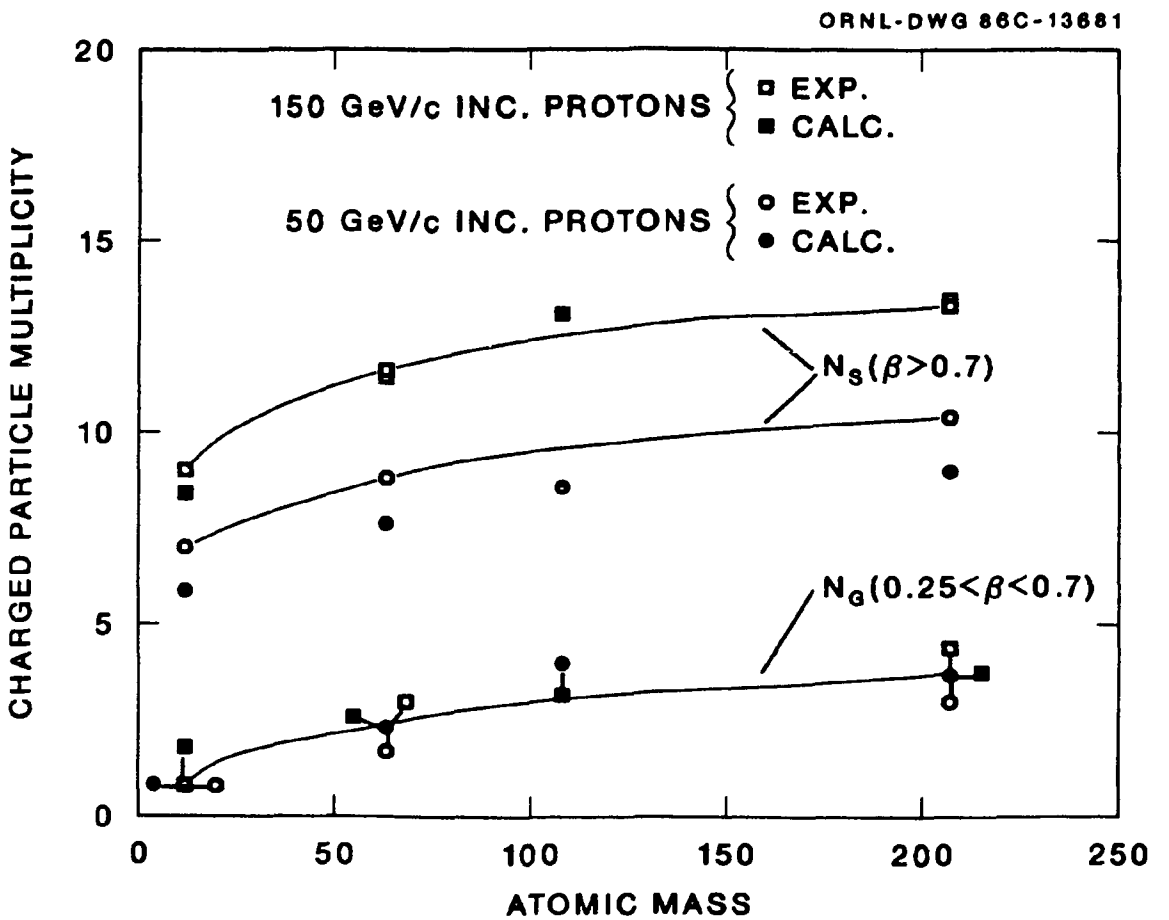

Figure 2. Average shower ($v/c \geq .7$) and grey ($.25 < v/c \leq .7$) charged particle multiplicities for 150 GeV/c and 50 GeV/c proton-silver collisions vs. atomic mass number.

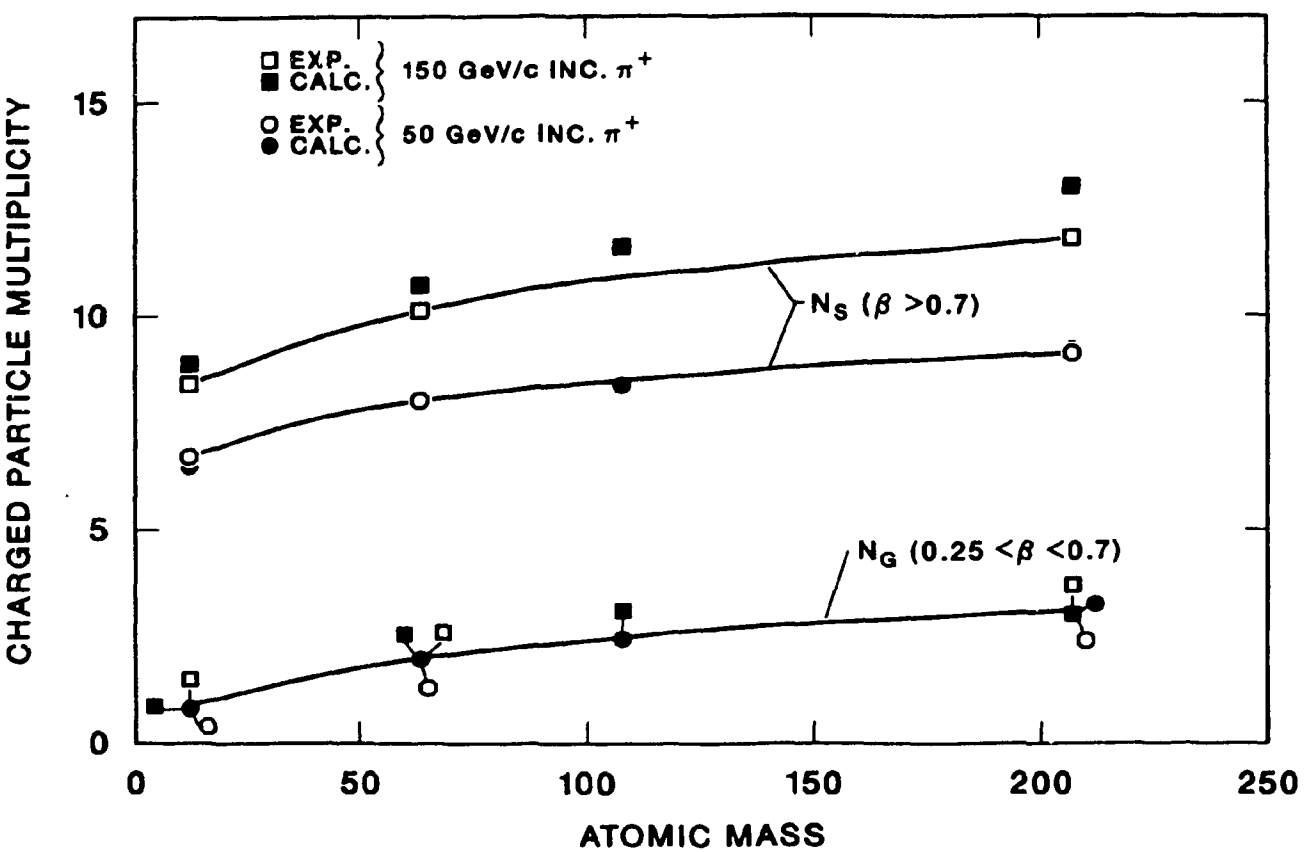

Figure 3. Average shower (v/c > .7) and grey (.25 < v/c ≤ .7) charged particle multiplicities for 150 GeV/c and 50 GeV/c pion$^+$-silver collisions vs. atomic mass number.

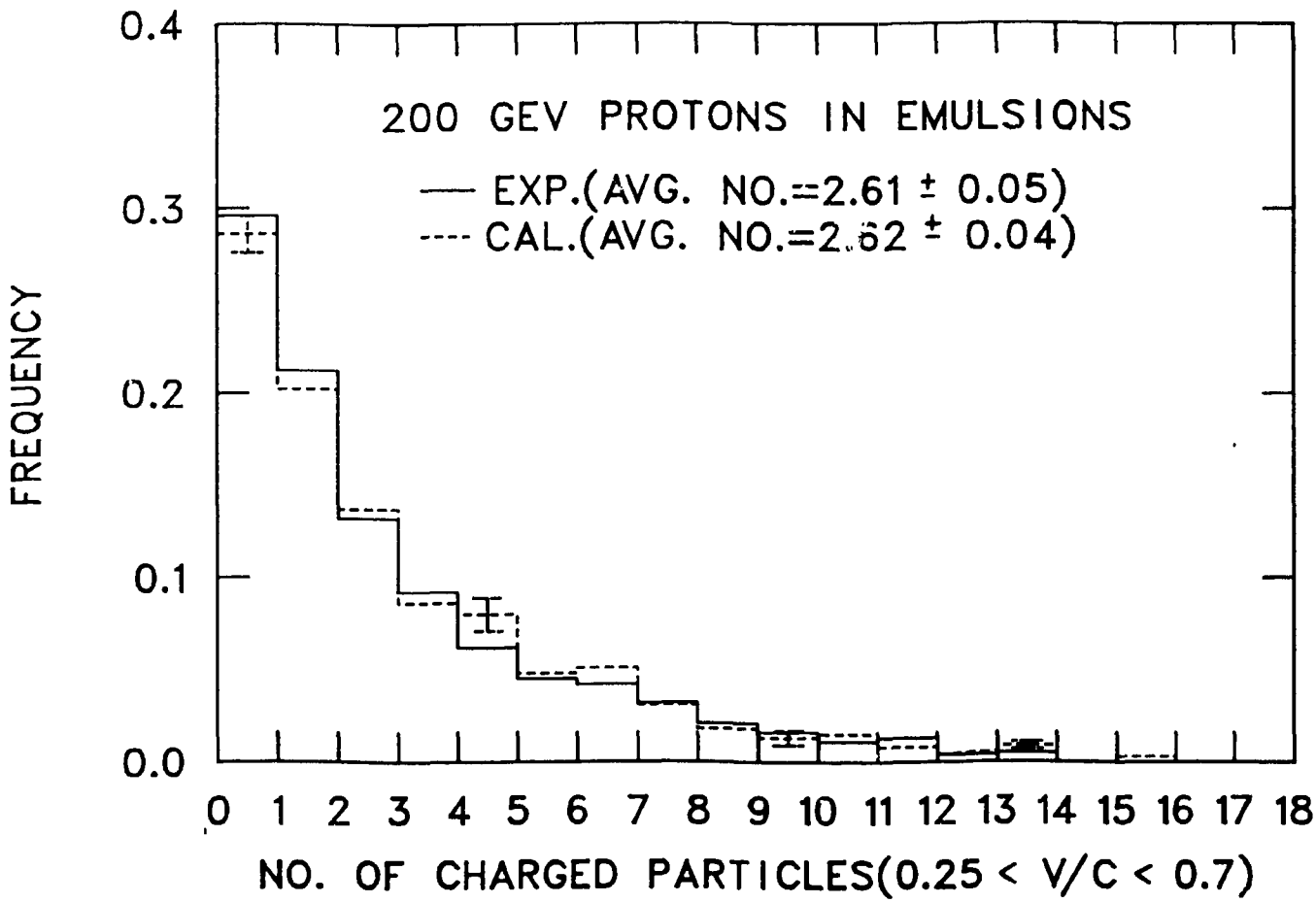

Figure 4. Frequency of the production of grey ($0.25 < v/c < 0.7$) charged particles for 200 GeV protons in emulsions.

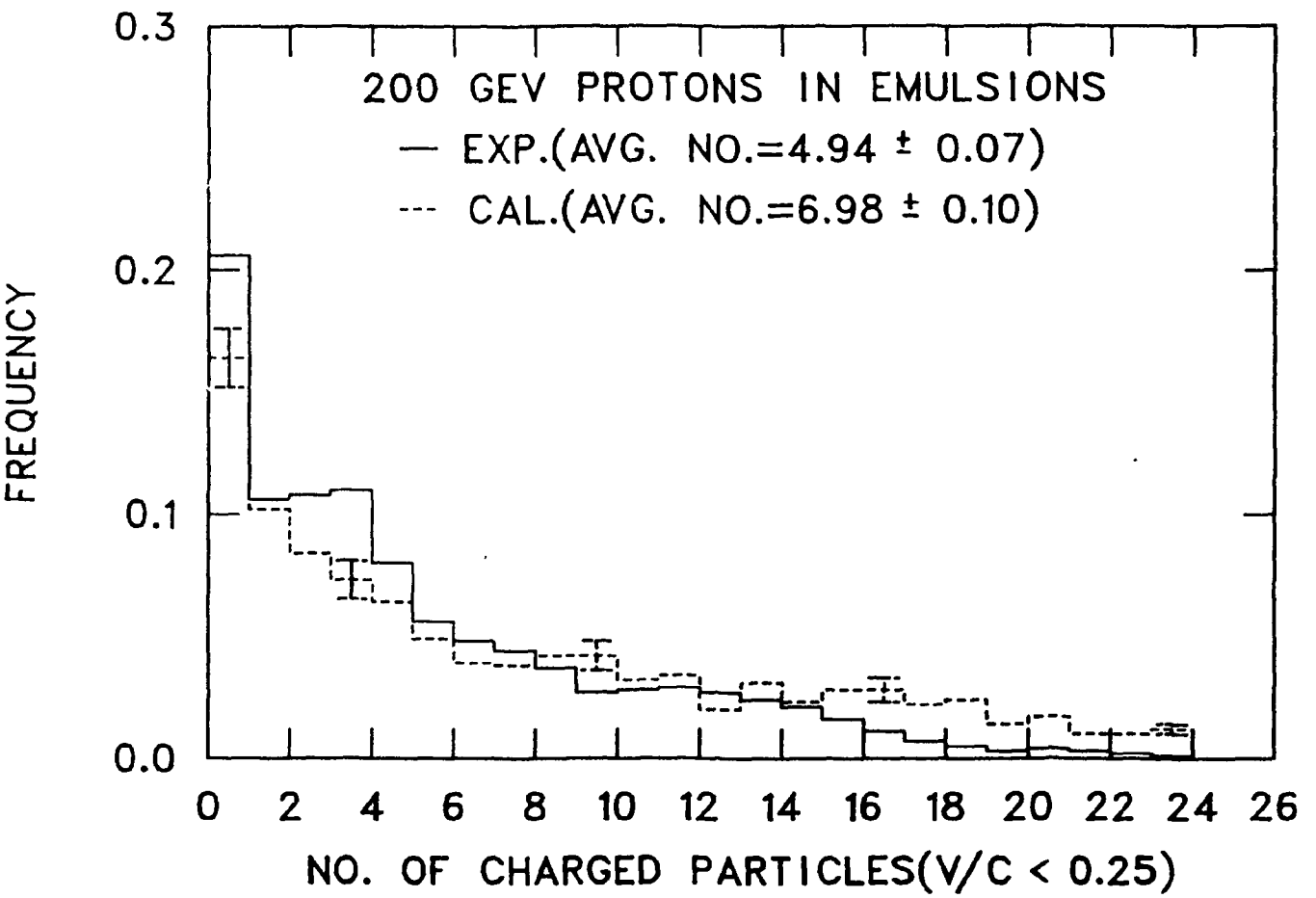

Figure 5. Frequency of the production of black ($v/c \leq 0.25$) charged particles for 200 GeV protons in emulsions.

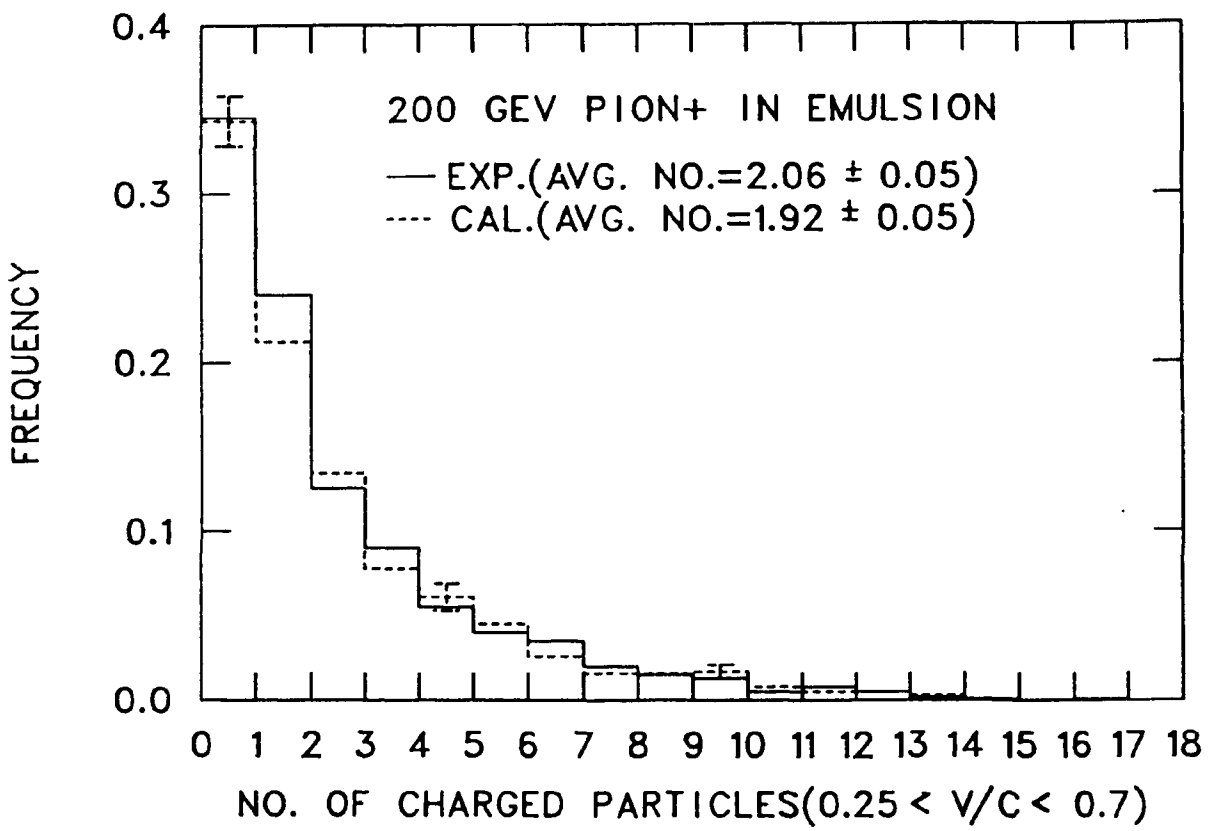

Figure 6. Frequency of the production of grey ($0.25 < v/c < 0.7$) charged particles for 200 GeV π^+ in emulsions.

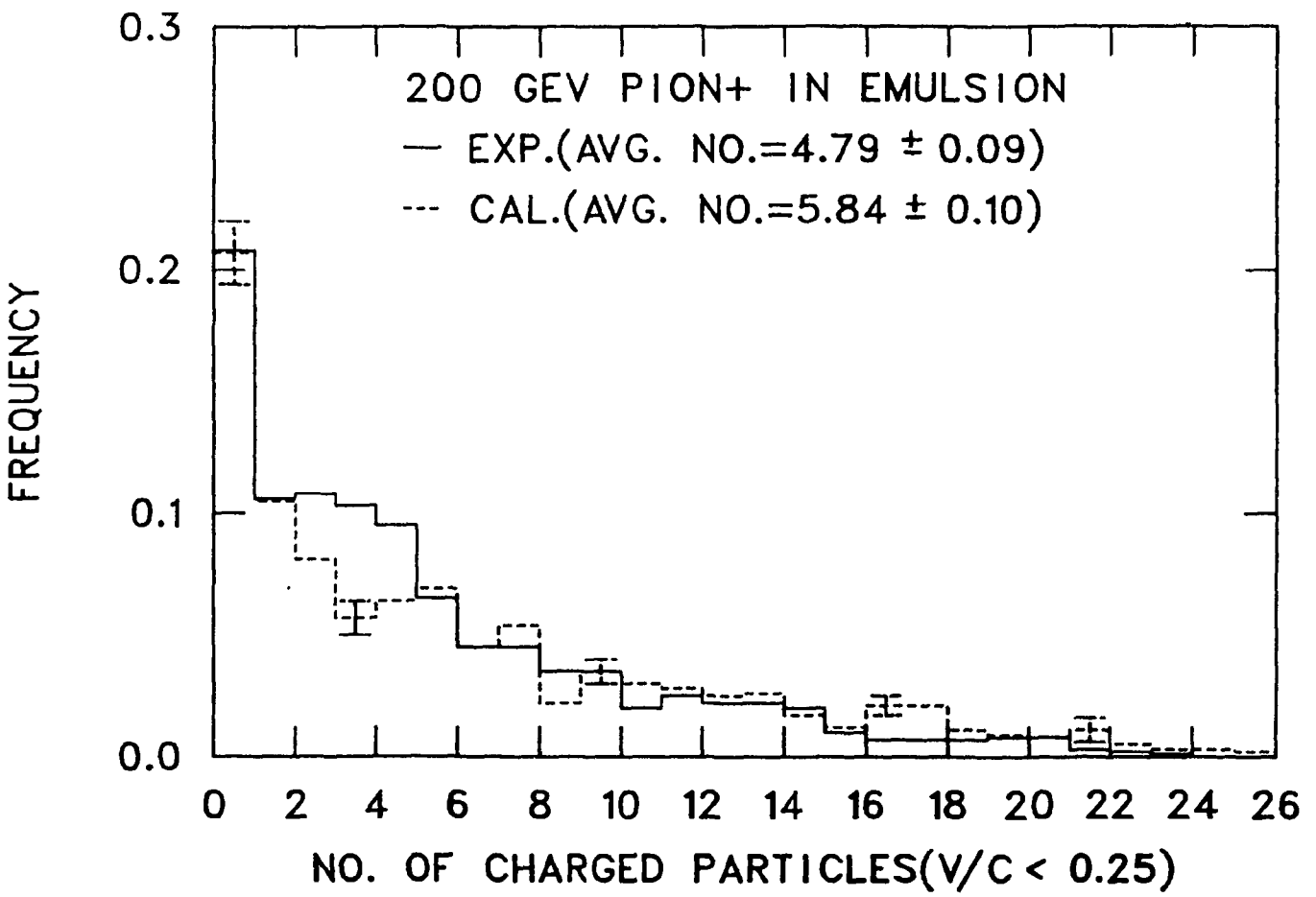

Figure 7. Frequency of the production of black ($v/c \leq 0.25$) charged particles for 200 GeV π^+ in emulsions.

For both incident protons and positively charged pions, the calculated and experimental distributions of grey charged particles agree very well. Thus, the model gives not only a reliable estimate of the average number of grey particles produced, but also reliably gives the fluctuations about the average. The good agreement is due to the correlations introduced, as shown by the similarity between Fig. 1 and Fig. 4.

The agreement between calculated and experimental data for black particles is generally close, but not as good as for grey particles. The calculated distributions are lower than the experimental data in the multiplicity range ν = 2-5 and are higher for $\nu > 16$. Consequently, the calculated averages exceed the experimental by one or two particles. This is not surprising since most of the black tracks are due to evaporation particles of energy less than a few MeV. The calculations include a small percentage of deuterons, tritons, ^{3}He, and alphas.

3.2 RESIDUAL NUCLEI MASS YIELD DISTRIBUTIONS

In Fig. 8 the measured partial cross sections for producing various residual nuclei are shown versus atomic mass number for 29 GeV proton-silver collisions.[11] Also shown in Fig. 8 are the calculated partial cross sections. The total cross section of 1172 mb used in the calculation is approximately equal to the value obtained experimentally by summing the partial cross sections for the production of all nuclei. In the figure, the error bars on the calculated results are statistical only and represent one standard deviation. Error bars are shown for only a few of the histogram values to avoid overcomplicating the figure. The calculated error bars where not shown are of the same order of magnitude as those shown. The agreement between the calculated and experimental data in Fig. 8 is quite good. In particular, the calculated results reproduce reasonably well the peak in the distribution at mass number near the target mass number. In Fig. 9 the measured[12] and calculated results are shown for 300 GeV proton-silver collisions. The total cross section was 1180 mb. The agreement is not as good at 300 GeV as at 29 GeV, but is still quite reasonable.

3.3 RAPIDITY

The rapidity of a secondary particle in the laboratory system is

$$y = 0.5 \; ln \left[\frac{E + P_{11}}{E - P_{11}} \right],$$

where E is the total energy and P_{11} the momentum component parallel to incoming projectile direction. In Fig. 10 the charged particle rapidity calculations for 200 GeV/c proton-argon collisions are compared with the data of DeMarzo et al.[13] The peaks at the left do not include all of the evaporation or any black particle contributions. Specifically, protons or heavy particles with momentum less than 200 MeV/c and mesons with momentum less than 35 MeV/c are omitted. The calculated histogram has a multiplicity of 13.6 particles, whereas the measured multiplicity is 15.0 particles. This difference reflects a difference in calculated and measured shower particle multiplicities of as much as 20% as shown also in Fig. 2.

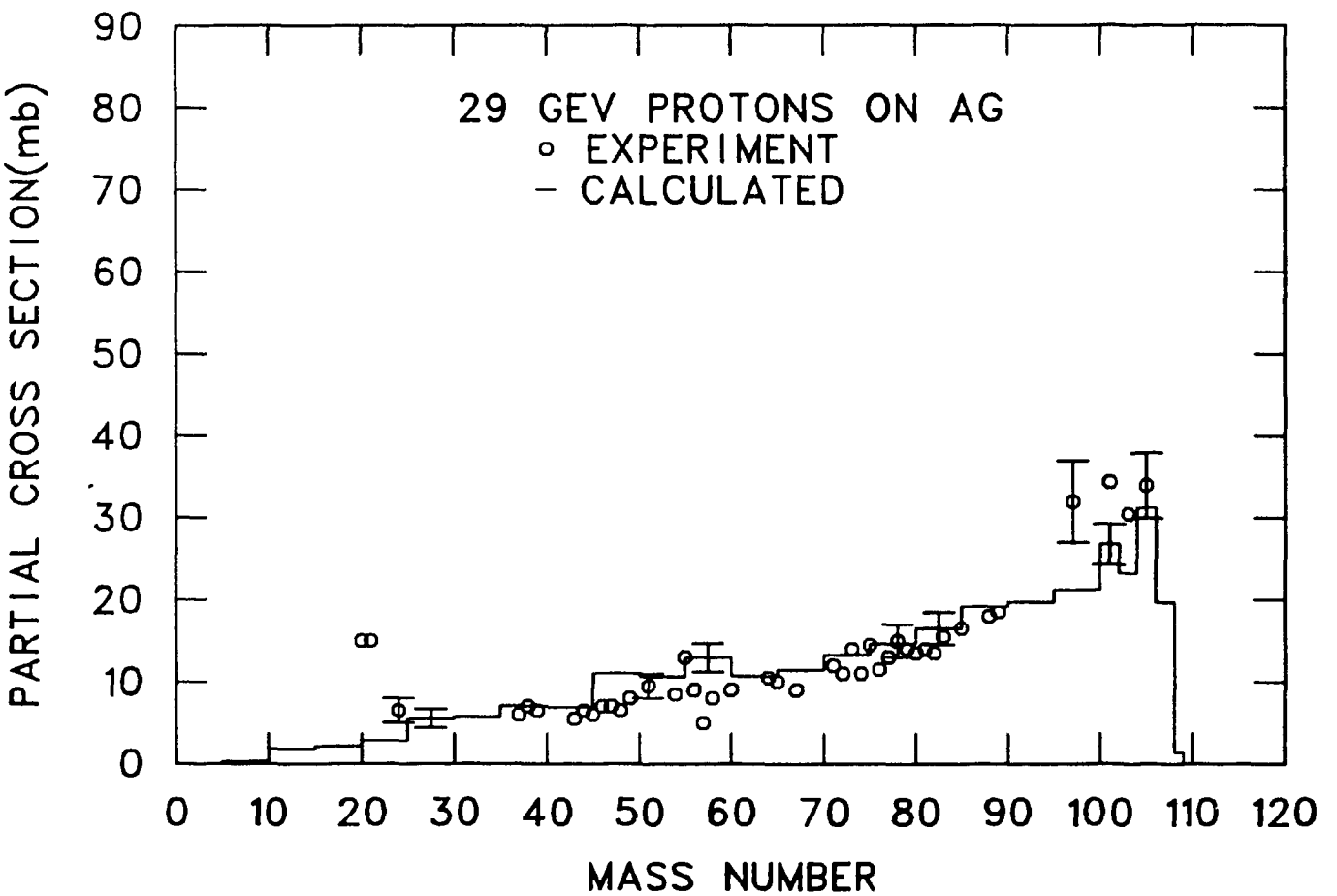

Figure 8. Partial cross sections vs. mass number for 29 GeV protons on silver.

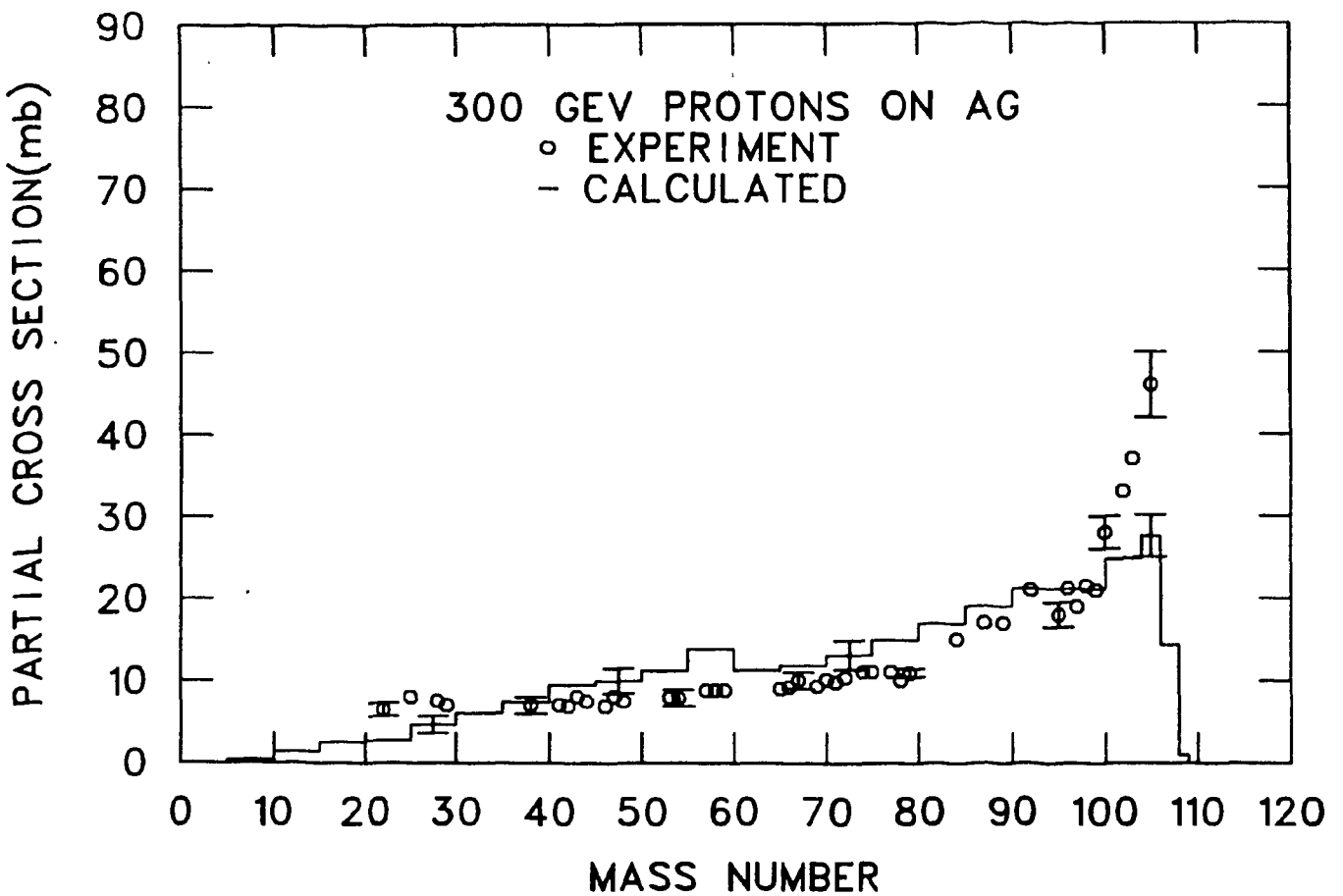

Figure 9. Partial cross sections vs. mass number for 300 GeV protons on silver.

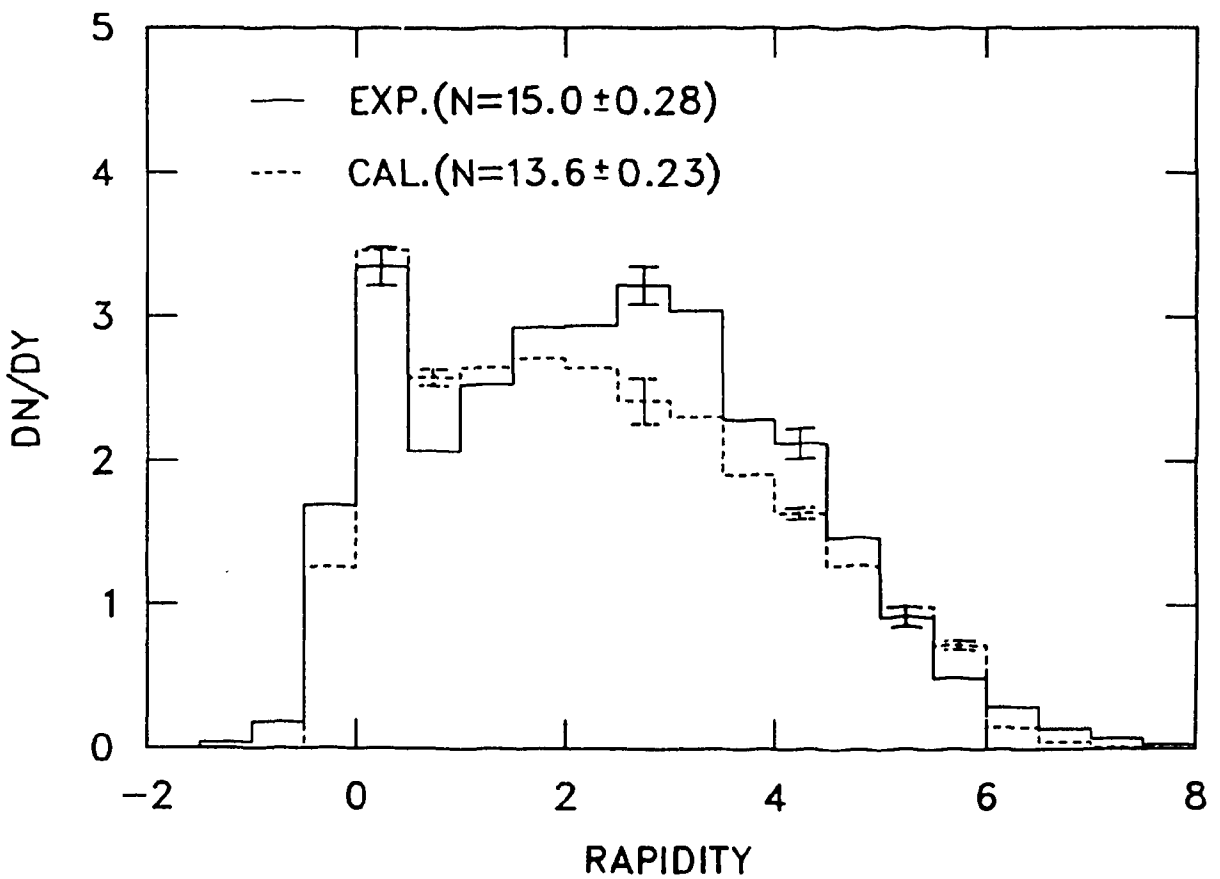

Figure 10. Rapidity spectrum for all charged particles for 200 GeV/c p-Argon collisions.

4. SUMMARY

The modifications introduced into the high-energy (5 GeV to 20 TeV) hadron-nucleus differential particle production model found in the Monte Carlo transport code FLUKA87, have been described and comparisons of calculated results obtained with the revised model and experimental data have presented. The modifications are primarily associated with the intranuclear cascade component of the hadron-nucleus collisions and are for the purpose of improving the agreement between the low energy (<400 MeV) produced particles and experimental data. With the revised model the frequency distributions of low energy ($\beta < 0.7$) charged particles as well as the multiplicities from hadron-nucleus collisions have been brought into better agreement with experimental data. Also, the distribution of residual nuclei from high-energy hadron-nucleus collisions are in much better agreement with experimental data. It should be noted that before the revisions were made the calculated residual nuclei distributions were in serious disagreement with experimental data.[8]

REFERENCES

1. T. A. Gabriel, F. S. Alsmiller, R. G. Alsmiller, Jr., B. L. Bishop, O. W. Hermann, and D. E. Groom, "Preliminary Simulations of the Neutron Flux Levels in the Fermilab Tunnel and Proposed SSC Tunnel," SSC Central Design Group Report, SSC-110, Lawrence Livermore National Laboratory (1987).

2. D. E. Groom, "Measurements and Simulations of the Neutron Foux in the Tevatron Tunnel," included in SSC Central Design Group Task Force Report, SSC-SR-1033, 163, Lawrence Livermore National Laboratory (1988).

3. J. Ranft and S. Ritter, "Rapidity Ratios, Feynman-X Distributions and Forward-Backward Correlations in Hadron-Nucleus Collisions in a Dual Monte Carlo Multi-Chain Fragmentation Model," *Z. Phys. C - Particles and Fields* **10**, 249 (1981).

4. A Capella and J. Tran. Thanh Van, "Hadron-Nucleus Interactions and The Leading Particle Effect in a Dual-Parton Model," *Z. Phys. C - Particles and Fields* **27**, 569 (1985).

5. R. G. Alsmiller, Jr., F. S. Alsmiller, T. A. Gabriel, and O. W. Hermann, "Modification of the High-Energy Transport Code (HETC) and Comparisons with Experimental Results," *Proc. of the ANS Topical Conference on the Theory and Practices in Radiation Protection and Shielding*, April 22-24, 1987, Knoxville, Tennessee.

6. R. G. Alsmiller, Jr., F. S. Alsmiller, T. A. Gabriel, O. W. Hermann, B. L. Bishop, "The Modified High-Energy Transport Code HETC and Design Calculations for the SSC," *Trans. Am. Nucl. Soc. 1988 Annual Meeting*, June 12-16, 1988, San Diego, California.

7. P. A. Aarnio, J. Lindgren, J. Ranft, A. Fasso, and G. R. Stevenson, "Enhancements to the FLUKA86 Program (FLUKA87)," CERN Divisional Report TIS-RP/190 (1987).

8. F. S. Alsmiller, R. G. Alsmiller, Jr., and O. W. Hermann, "Low-Energy Particle Production and Residual Nuclei Production in High-Energy Hadron-Nucleus Collisions," *Proc. of the ANS Topical Conference on the Theory and Practice in Radiation Protection and Shielding*, April 22-24, 1987, Knoxville, Tennessee.

9. J. Babecki and G. Nowak, "Characteristics of Slow Particles in Hadron-Nucleus Interactions and Their Relation to the Models of High Energy Interactions," *Acta Physica Polonica* **B9**, 5 (1978).

10. M. A. Faessler, "New Experimental Results for Particle Production from Nuclei," *Annals of Physics* **137**, 44 (1981).

11. S. Katcoff, H. R. Fickel, and A. Wyttenbach, "Distribution of Radionuclides from the Interaction of 3- and 29-GeV Protons with Silver," *Phys. Rev.* **166**, 4 (1968).

12. N. T. Porile, G. D. Cole and C. R. Rudy, "Nuclear Reactions of Silver with 25.2 GeV ^{12}C Ions and 300 GeV Protons," *Phys. Rev. C* **19**, 6 (1979).

13. C. DeMarzo et al., "Multiparticle Production on Hydrogen, Argon, and Xenon Targets in a Streamer Chamber by 200 GeV/c Proton and Antiproton Beams," *Phys. Rev. D* **26**, 5 (1982).

14. G. Nilsson and E. Stenlund, Lund University preprint, LU-TP80-9 (1980).

15. See Appendices A, B, and C.

16. H. W. Bertini, "Nonelastic Interactions of Nucleons and π Meson with Complex Nuclei at Energies Below 3 GeV," *Phys. Rev* **C6**, 631 (1972).

17. J. Ranft and S. Ritter, *Z. Phys. C - Particles and Fields* **27**, 569 (1985).

18. A. M. Wapstra, *Physica* **21**, 367 (1955).

19. M. P. Guthrie, "EVAP-2 and EVAP-3: Modifications of a Code to Calculate Particle Evaporation from Excited Compound Nuclei," ORNL-4379 (1969); M. P. Guthrie, "EVAP-4: Another Modification of a Code to Calculate Particle Evaporation from Excited Compound Nuclei," ORNL/TM-3119 (1970).

20. J. Ranft, CERN TIS Divisional Report TIS-RP/172/PP (1986). P. A. Aarnio, *Z. Phys. C - Particles and Fields* **23**, 67 (1984).

21. J. Ranft and S. Ritter, "Particle Production in Hadron-Nucleus Collisions in a Multi-Chain Fragmentation Model," *Z. Phys. C - Particles and Fields* **20**, 347 (1983).

22. Ilford Nuclear Research Emulsions (Ilford Research Lab., Ilford, London, England, 1949).

23. J. Ranft and J. T. Routti, "Hadronic Cascade Calculations of Angular Distributions of Integrated Secondary Particle Fluxes From External Targets and New Empirical Formulae Describing Particle Production in Proton-Nucleus Collisions," Part. Accel. 4, 101 (1972).

APPENDIX A

The expressions for the average total kinetic energy, expended on intranuclear cascade nucleons) are taken from the functions called by subroutine EVENTQ in the transport code FLUKA87 (see also Ref. 23). If A_T is the target nucleus atomic number and E the projectile kinetic energy,

$$E_{Co} = 2.5 A_T^2 f_N f_A f,$$

where, for $E \geq 10$ GeV,

$$\begin{aligned} f_N &= 0.1104 && \text{protons,} \\ &= 0.190 && \text{neutrons.} \end{aligned}$$

For $E < 10$ GeV, and $IT = 1$ or 2,

$$f_N = 0.5 + A(IT)[1.0 + (\log_{10} E)^2]D(IT)$$

$$\begin{aligned} A(1) = 1.0; D(1) = 0.14 && \text{protons,} \\ A(2) = 1.3; D(2) = 0.19 && \text{neutrons,} \end{aligned}$$

$$f_A = f_E(1.0 - 0.001 A_T),$$

where, for $E > 10$ GeV,

$$\begin{aligned} f_E &= .21 && \text{protons,} \\ &= .20 && \text{neutrons,} \end{aligned}$$

and, for $E \leq 10$ GeV,

$$\begin{aligned} f_E &= 0.11 + 0.01E && \text{protons,} \\ &= 0.10 + 0.01E && \text{neutrons.} \end{aligned}$$

If $E \geq 5.0\ f_A$,

$$f = 1.0.$$

If $E < 5.0\ f_A$,

$$f = \frac{[1.0 - (1.0 + E/f_A)\exp(-E/f_A)]}{[1.0 - \exp(-E/f_A)]}.$$

For $E < 125$ MeV,

$$E_{Co} = 0.0.$$

The kinetic energies are sampled from

$$E = -f_A ln(R),$$

where R is a random number between 0.0 and 1.0.

APPENDIX B

The fractions used in Eq. (2) to multiply the average total kinetic energy given to intranuclear cascade nucleons are given in Table B.1 for incoming baryons and in Table B.2 for incoming mesons.

Table B.1
The fraction multiplying E_{CO}, the average total kinetic energy given to intranuclear cascade nucleons for incoming baryons on target nucleus A_T

A_T	Fract	A_T	Fract	A_T	Fract
1-12	0.25	44	0.61	76	0.805
13	0.26	45	0.62	77	0.810
14	0.28	46	0.63	78	0.812
15	0.29	47	0.635	79	0.815
16	0.30	48	0.64	80	0.82
17	0.315	49	0.65	81	0.822
18	0.33	50	0.66	82	0.824
19	0.34	51	0.67	83	0.825
20	0.35	52	0.675	84	0.825
21	0.36	53	0.68	85	0.83
22	0.38	54	0.69	86	0.832
23	0.39	55	0.70	87	0.834
24	0.40	56	0.71	88	0.836
25	0.41	57	0.715	89	0.838
26	0.42	58	0.72	90	0.840
27	0.43	59	0.725	91	0.843
28	0.44	60	0.73	92	0.836
29	0.46	61	0.735	93	0.849
30	0.47	62	0.74	94	0.852
31	0.48	63	0.75	95	0.855
32	0.49	64	0.755	96	0.856
33	0.50	65	0.76	97	0.857
34	0.51	66	0.767	98	0.858
35	0.52	67	0.77	99	0.859
36	0.53	68	0.77	100	0.86
37	0.54	69	0.775	101	0.862
38	0.55	70	0.78	102	0.864
39	0.56	41	0.783	103	0.866
40	0.57	72	0.786	104	0.868
41	0.58	73	0.79	105	0.870
42	0.59	74	0.795	106	0.872
43	0.60	75	0.80	107	0.874

If $108 \leq A_T$ 206,

$$Fract_{baryon} = 0.739 + 1.26 \times 10^{-3} \cdot A_T.$$

If $207 \leq A_T \leq 250$,

$$Fract_{baryon} = 1.0.$$

The fractions for incoming mesons are given in Table B.2.

Table B.2
Incoming Mesons

A_T	Fract	A_T	Fract	A_T	Fract
1-12	0.25	30	0.415	48	0.505
13	0.262	31	0.420	49	0.510
14	0.274	32	0.425	50	0.515
15	0.285	33	0.430	51	0.519
16	0.295	34	0.435	52	0.523
17	0.305	35	0.44	53	0.526
18	0.315	36	0.446	54	0.520
19	0.327	37	0.452	55	0.533
20	0.34	38	0.458	56	0.537
21	0.345	39	0.464	57	0.54
22	0.35	40	0.47	58	0.543
23	0.36	41	0.474	59	0.547
24	0.37	42	0.478	60	0.55
25	0.38	43	0.482	61	0.555
26	0.385	44	0.486	62	0.559
27	0.39	45	0.49	63	0.5625
28	0.398	46	0.495		
29	0.406	47	0.50		

If $64 \leq A_T \leq 250$,

$$Fract_{meson} = 0.75\ Fract_{baryon}.$$

APPENDIX C

Table C.1 gives the frequency of errors in total energy conservation in the lab system inside the cutoff well for 200 GeV/c p-Argon collisions. The total number of histories was 2500. All collisions for which the error in conservation for any four-momentum component was greater than two percent in the target nucleon rest system were rejected and recalculated, so are missing from this table. The total number of such rejections was 35, or 1.4%. The errors shown in the table can possibly be explained as due to the use of single precision. Small errors in the rest systems of decaying resonances are greatly augmented by the Lorentz transformations at high energies.

Tables C.2 and C.3 give the frequency of errors in momentum conservation. The errors are much larger because the selection process for intranuclear cascade nucleons does not conserve momentum.

Table C.1

Frequency of Errors in Total Energy Conservation
200 GeV/c p-Argon Collisions

Error (MeV)	Frequency	Error (MeV)	Frequency
5.0	1,278	-5.0	359
10.0	70	-10.0	80
15.0	48	-15.0	58
20.0	48	-20.0	41
25.0	38	-25.0	28
30.0	37	-30.0	24
35.0	30	-35.0	25
40.0	28	-40.0	20
45.0	20	-45.0	20
50.0	16	-50.0	17
55.0	15	-55.0	14
60.0	11	-60.0	15
65.0	9	-65.0	12
70.0	7	-70.0	12
75.0	5	-75.0	7
100.0	25	-100.0	14
200.0	17	-200.0	31
250.0	0	-250.0	2

Table C.2

Frequency of Errors in Longitudinal Momentum Conservation
200 GeV/c p-Argon Collisions

Error (MeV/c)	Frequency	Error (MeV/c)	Frequency
100	151	-100	150
200	131	-200	119
300	139	-300	112
400	146	-400	115
500	118	-500	90
600	121	-600	82
700	120	-700	73
800	102	-800	55
900	85	-900	37
1000	65	-1000	40
1100	64	-1100	31
1200	57	-1200	27
1300	42	-1300	15
1400	39	-1400	14
1500	32	-1500	7
1600	18	-1600	5
1700	16	-1700	2
1800	10	-1800	3
1900	13	-1900	1
2000	7	-2000	2
2100	12	-2100	0
2200	8	-2200	2
3000	20	-3000	0

Table C.3

Frequency of Errors in Transverse Momentum Component Conservation 200 GeV/c p-Argon Collisions

Error (MeV/c)	Frequency	Error (MeV/c)	Frequency
100	155	-100	142
200	168	-200	144
300	146	-300	146
400	134	-400	163
500	127	-500	113
600	116	-600	100
700	79	-700	101
800	72	-800	81
900	56	-900	60
1000	55	-1000	43
1100	38	-1100	47
1200	28	-1200	25
1300	20	-1300	27
1400	22	-1400	20
1500	13	-1500	8
1600	8	-1600	5
1700	8	-1700	7
1800	5	-1800	5
1900	3	-1900	5
2000	3	-2000	4

INTERNAL DISTRIBUTION

1. F. S. Alsmiller
2. R. G. Alsmiller, Jr.
3. B. R. Appleton
4. D. E. Bartine
5. B. L. Bishop
6–10. T. A. Gabriel
11. D. T. Ingersoll
12. J. K. Ingersoll
13. R. A. Lillie
14. F. C. Maienschein
15. RSIC
16. C. Zeigler
17. EPMD Reports Office
18–19. Laboratory Records Department
20. Laboratory Records, ORNL-RC
21. Document Reference Section
22. Central Research Library
23. ORNL Patent Section

EXTERNAL DISTRIBUTION

24. Office of Assistant Manager, for Energy Research and Development, Department of Energy, Oak Ridge Operations, P.O. Box 2001, Oak Ridge, TN 37831

25–34. Office of Scientific and Technical Information, P.O. Box 62, Oak Ridge, Tennessee 37830

35. Argonne National Laboratory, Library Services Dept., 302-CE125, 9700 S. Cass Avenue, Argonne, IL 60439
36. T. W. Armstrong, Science Applications, Inc., PO Box 2807, La Jolla, CA 92038
37. Miguel Awschalom, National Accelerator Laboratory, PO Box 500, Batavia, IL 60510
38. V. S. Barashenkov, Laboratory of Theoretical Physics, Joint Institute for Nuclear Research, Head Post Office, PO Box 79, Moscow, USSR
39. Gerald W. Bennett, Brookhaven National Laboratory, Upton, NY 11973
40. D. Berley, National Science Foundation, Washington, DC 20550
41. Elliott Bloom, Stanford Linear Accelerator Center, PO Box 4349, Stanford, CA 94305

42–46. J. Brau, University of Oregon, Eugene, OR 97403

47. Bruce Brown, Fermi National Accelerator Laboratory, PO Box 500, Batavia, IL 60510
48. David O. Caldwell, Dept. of Physics, University of California, at Santa Barbara, Santa Barbara, CA 93106
49. Stanley B. Curtis, Lawrence Radiation Laboratory, Bldg. 29, Room 213, Berkeley, CA 94720
50. Herbert DeStaebler, Stanford Linear Accelerator Center, Stanford University, Stanford, CA 94305
51. A. DiCiaccio, CERN, Geneva 23, Switzerland
52. J. J. Dorning, Dept. of Nucl. Eng., and Engineering Physics, University of Virginia, Charlottesville, VA 22901
53. R. D. Edge, Physics Department, University of South Carolina, Columbia, SC 29208
54. R. Eisenstein, Department of Physics, University of Illinois, Urbana, IL 61801
55. R. W. Ellsworth, George Mason University, Fairfax, VA 22030

56. Chris Fabjan, CERN, Geneva 23, Switzerland
57. G. Feldman, Stanford Linear Accelerator Center, Stanford University, Stanford, CA 94305
58. W. T. Ford, Experiment 1A-Lab C, Fermi National Accelerator Laboratory, PO Box 500, Batavia, IL 60510
59. E. Fowler, Department of Physics, Purdue University, West Lafayette, IN 47907
60. H. T. Freudenreich, University of Maryland, College Park, MD 20742
61. E. Freytag, Deutsches Elektronen-Synchrotron, DESY, 2 Hamburg Drive, Flottbek, Notkesteig 1, West Germany
62. M. G. D. Gilchriese, SSC Central Design Group, Lawrence Berkeley Laboratory, Berkeley, CA 94720
63. G. T. Gillies, Department of Physics, University of Virginia, Charlottesville, VA 22901
64. G. E. Gladding, University of Illinois, Department of Physics, Urbana, IL 61801
65. K. Goebel, Health Physics Group, CERN, 1211 Geneva 23, Switzerland
66. J. A. Goodman, University of Maryland, College Park, MD 20742
67. M. Goodman, Bell Communication Research, Morristown, NJ 07960
68. D. Groom, SSC Central Design Group, Lawrence Berkeley Laboratory, Berkeley, CA 94720
69. Herman Grunder, Deputy Director, General Sciences, Lawrence Berkeley Laboratory, 1 Cyclotron Rd, Berkeley, CA 94720
70. H. J. Hargis, University of Tennessee, Department of Physics, Knoxville, TN 37919
71. Frenc Hajnal, Health and Safety Laboratory, U.S. Department of Energy, 376 Hudson St, New York, NY 120014
72. R. M. Haralick, Department of Electrical Engineering, University of Washington, Seattle, WA 98195
73. M. Hofert, CERN, 1211 Geneva 23, Switzerland
74. Terrence Jensen, Department of Physics & Astronomy, The University of Rochester, Rochester, NY 14726
75. D. Lal, Tata Institute of Fundamental Research, National Centre of the Government of India, for Nuclear Science & Mathematics, Homi Bhabha Rd, Bombay 5, India
76. Lawrence Livermore Laboratory, Technical Information Department, PO Box 808, Livermore, CA 94550
77. V. Lebedev, Institute of High Energy Physics, Serpukhov, Moscow Region, USSR
78. Library for Nuclear Science, Massachusetts Institute of Technology, at Middleton, Middleton, MA 01949
79. J. LoSecco, Department of Physics, California Institute of Technology, Pasadena, CA 91125
80. J. Marks, Accelerator Fusion Research Division, Lawrence Berkeley Laboratory, 1 Cyclotron Rd, Berkeley, CA 94720
81. A. I. Mincer, University of Maryland, College Park, MD 20742
82. V. S. Narashimham, Tata Institute of Fundamental Research, Bombay 400 005, India
83. W. R. Nelson, Stanford Linear Accelerator Center, Stanford University, PO Box 4349, Stanford, CA 94305

84. T. R. Palfrey, Jr., Department of Physics, Purdue University, West Lafayette, IN 47907
85. Robert Palmer, Brookhaven National Laboratory, Upton, NY 11973
86. C. W. Peck, Department of Physics, California Institute of Technology, Pasadena, CA 91109
87. J. Ranft, Karl-Marx University, Physics Section, Linnestrasse 5,701, Leipzig, East Germany
88. Lincoln Read, Division of High Energy, and Nuclear Physics, Department of Energy, Washington, DC 20545
89. Jim Reidy, University of Mississippi, University, MS 38677
90. C. Rubbia, Lyman Laboratory, Harvard University, Cambridge, MA 02138
91. W. Schmidt, Institute of Experimental Nucl. Phys., University of Karlsruhe, 75 Karlsruhe, West Germany
92. The Secretary, Radiation Group, Lab II, CERN, 1211 Geneva 23, Switzerland
93. Walter Selove, University of Pennsylvania, Department of Physics, Philadelphia, PA 19104
94. B.S.P. Shen, Department of Astronomy, University of Pennsylvania, Philadelphia, PA 19104
95. M. Shupe, Department of Physics, University of Minnesota, Minneapolis, MN 55455
96. Alan Stevens, Physics Department, Brookhaven National Laboratory, Upton, NY 11973
97. G. R. Stevenson, Radiation Protection Group, Lab II, CERN, 1211 Geneva 23, Switzerland
98. L. Sulak, Department of Physics, University of Michigan, Ann Arbor, MI 48109
99. R. F. Taschek, Los Alamos National Laboratory, PO Box 1663, Los Alamos, NM 87544
100. R. Tesch, DESY, Hamburg, Notkesteig 1, West Germany
101. R. H. Thomas, Lawrence Radiation Laboratory, Health Physics Department, Bldg. 72, Berkeley, CA 94720
102. V. D. Toneev, Laboratory of Theoretical Physics, Joint Institute for Nuclear Research, Head Post Office, PO Box 79, Moscow, USSR
103. S. C. Tonwar, University of Maryland, College Park, Md 20742
104. W. Turchinetz, Massachusetts Institute of Technology, R26-411, Cambridge, MA 02139
105. Jim Walker, University of Florida, Gainesville, FL 32611
106. W. J. Willis, CERN, Geneva 23, Switzerland
107. D. Winn, Lyman Laboratory, Harvard University, Cambridge, MA 02138
108. J. Wilczynski, Nuclear Research Center, Karlsruhe, West Germany
109. S. Yellin, Stanford University, Stanford Linear Accelerator Center, PO Box 4349, Stanford, CA 94305
110. G. B. Yodh, University of Maryland, College Park, Md 20742
111. S. Youssef, SCRI, Florida State University, Tallahassee, FL 32306
112. B. Zeitnitz, Nuclear Research Center, Karlsruhe, West Germany